Bull Earthquake Eng (2014) 12:1221–1237
DOI 10.1007/s10518-013-9553-1

ORIGINAL RESEARCH PAPER

Kinematic interaction of piles in laterally spreading ground

George Bouckovalas · Yannis Chaloulos

Received: 17 December 2012 / Accepted: 2 November 2013 / Published online: 22 November 2013

Abstract All current empirical approaches for pile design in liquefied soils agree that the ultimate soil pressure on the pile is drastically reduced relative to the reference ultimate pressures, in the absence of liquefaction. However, there is disagreement with regard to the extent of the aforementioned reduction and also controversy about the pile and soil parameters which control it. For instance, well documented experimental data from centrifuge tests show that significant negative excess pore pressures may develop due to the dilation of the liquefied soil that flows around the upper part of the pile, thus enhancing ultimate soil pressures well above the recommended values. In view of the above objective uncertainties, the problem was analyzed numerically using a 3D dynamic procedure. Namely, FLAC 3D was combined with the NTUA Sand constitutive model, for dynamic loading and liquefaction of cohesionless soils, and was consequently used to perform parametric analyses for various pile, soil and seismic excitation characteristics. To ensure the validity of the predictions, the numerical methodology was first verified against the afore mentioned centrifuge experiments. It is thus concluded that dilation-induced negative excess pore pressures are indeed possible for common pile and soil conditions encountered in practice. As a result, apart from the relative density of the sand, a common parameter in most empirical relations, a number of other dilation related factors influence also the ultimate soil pressure, such as: the effective confining stress, the permeability of the sand and the predominant excitation period, as well as the pile diameter and deflection. Furthermore, it is shown that dilation effects are more pronounced at the upper and middle segments of the pile, having an overall detrimental effect on pile response. Finally, a preliminary evaluation of numerical results shows that the development of a new methodology for the evaluation of p–y response in laterally spreading soils which would incorporate the above effects is feasible.

Keywords Single piles · Lateral spreading · Liquefaction · p–y Relations · 3D numerical analysis

G. Bouckovalas · Y. Chaloulos (✉)
School of Civil Engineering, NTUA, Athens, Greece
e-mail: ioannischaloulos@gmail.com

1 Problem outline

The current design practice for piles subjected to horizontal loads is largely based on the "Beam on Nonlinear Winkler Foundation" (BNWF) method, alternatively known as the p–y method. Possibly, the most uncertain parameter involved in the above formulation, is the determination of the non-linear force-displacement relationship for the Winkler springs, widely known as the "p–y curves". In a typical BNWF analysis, the characteristics of the p–y curves differ depending on the soil type in which the pile is built, as well as on the type of loading applied to the pile. As far as soil types are concerned, we can distinguish between cohesive and cohesionless soils, while the latter can be either non-liquefied (hereafter referred as "dry") or liquefied. As for the different types of loads imposed to the pile, these can be either kinematic (caused by lateral ground displacement) or external (forces and moments applied at the pile head by the superstructure). Furthermore, external loads can be either static or dynamic, while kinematic loads can be either transient or permanent. Among the above different soil and loading combinations, the present paper deals with the case of p–y curves for piles in "liquefied" sand, subjected to kinematic loads caused by permanent ground displacement due to lateral spreading.

Given the importance of p–y curves on the design of the pile, it is no surprise that a large number of research studies have been dedicated to this topic, and have given valuable insight to the parameters that affect the p–y curves. However, recent experimental data raise a number of reasonable concerns which are briefly outlined below:

a. Existing methodologies for estimating the liquefied p–y response are based on the corresponding relations for "dry sands" after properly *reducing* the ultimate soil pressure and the initial subgrade modulus. Modification of the curves for "dry sands" is performed either by applying appropriate reduction factors (e.g. Brandenberg et al. 2007) or by considering empirical relations for the residual strength of liquefied soil (e.g. Cubrinovski and Ishihara 2007). In both cases, the pursued reduction of the p–y curves is essentially related to the relative density of the sand alone.
b. Contrary to the above, recent experimental data (e.g. Tokimatsu and Suzuki 2009) indicate the influence of additional parameters like soil permeability, excitation characteristics, as well, as pile properties (bending stiffness, installation, head constraint, e.t.c.). Along the same direction, González et al. (2009) have shown that significant negative excess pore pressures may develop near the pile head, for values of soil permeability commonly encountered in the field, thus increasing instead of decreasing the soil pressures compared to the non-liquefied case.

The preceding discussion reveals that the problem under consideration deserves further investigation. Nevertheless pursuing this challenge purely by experimental means may prove technically and financially cumbersome since the number of parameters involved is large and the required number of experiments will be equally large. On the other hand, recent advances in numerical methods, along with the development of sophisticated constitutive models for soil response under even extreme conditions (e.g. earthquake–induced liquefaction), provide alternative means to overcome this limitation, through parametric analyses with a realistic numerical model. To this extent, the p–y response of piles undergoing lateral spreading displacements is investigated herein through a series of "numerical experiments", i.e. advanced numerical analyses which take consistently into account dynamic loading, excess pore pressure build up and drainage, as well as non-linear soil response.

In this context, the scope of the present paper is (a) to present details of an advanced 3D numerical methodology for the simulation of piles in "liquefied" sands, undergoing kinematic

loads due to permanent ground displacement, and (b) consequently apply the aforementioned methodology in order to investigate the mechanisms that govern the pile response and define the associated basic soil, pile and excitation parameters.

2 Numerical simulation of piles in laterally spreading soils

The model used for the simulation of the problem at hand is illustrated in Fig. 1. A single pile is built within a uniform, fully saturated and slightly inclined layer of fine Nevada sand. The inclination of the ground surface is simulated as a horizontal gravitational acceleration component, while contact (slip and separation) elements are used to simulate the pile–soil interface. A sinusoidal motion is applied at the base of the model, causing large kinematic loads on the pile due to soil liquefaction and lateral spreading. The corresponding p–y curves are consequently obtained from the normal and shear stresses developing at the nodes of the interface elements.

In total, eighteen (18) parametric analyses were performed for different soil, pile and excitation characteristics. Namely, the soil relative density varied between $D_r = 35$ and 70 %, the soil permeability varied between $k = 6.1e{-}5$ and $1.8e{-}3$ m/s, the pile diameter varied between $D = 0.40$ and 0.80 m, the bending stiffness varied between $EI = 2.5e5$ and $9.75e6\,kNm^2$, while the excitation period varied between $T = 0.20$ and 0.50 s. When one of the above problem parameters varied, all the rest were kept equal to the reference values ($D_r = 50$ %, $k = 6.1e{-}5$ m/s, $D = 0.60$ m, $EI = 1.3e6\,kNm^2$ and $T = 0.30$ s). Note that the analyses exploring the effects of diameter were performed by scaling proportionally all mesh dimensions in Figure 1. The piles were drilled (reference case) or driven, while the pile head was assumed to be free (reference case), rigidly fixed or with restricted rotation.

The numerical analyses are performed with the Finite Difference Code FLAC3D v.4.0. The major advantage of this code is that it allows coupling between pore water flow and dynamic loading, while it makes use of an explicit integration algorithm, which is more efficient for highly non-linear dynamic problems (e.g. pore water flow, liquefaction). In addition, through its user-defined-model (UDM) option, it allows for the implementation of sophisticated constitutive models for the accurate simulation of soil response. In this context, the advanced constitutive model NTUA Sand (Papadimitriou and Bouckovalas 2002; Andrianopoulos et al. 2010), as implemented to FLAC3D by Karamitros (2010), was used.

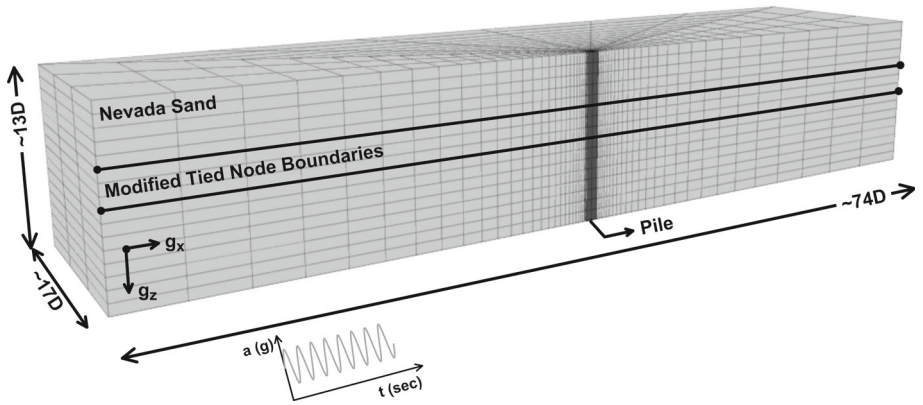

Fig. 1 3D numerical model of a single pile in laterally spreading ground

The specific model incorporates the Critical State Theory of Soil Mechanics, so that the effects of initial state (relative density and mean effective stress) are simulated with one single set of parameters. Furthermore, the Ramberg–Osgood formulation is adopted for elastic strain increments, allowing for the accurate simulation of the non-linear hysteretic response of sands (decrease of shear modulus and increase of hysteretic damping with increasing cyclic shear strain amplitude) at all strain levels. Finally, the plastic modulus formulation takes into account the effects of fabric evolution, leading to realistic simulation of shake-down effects and liquefaction during cyclic loading.

The well-known "tied node" method (e.g. Ghosh and Madabhushi 2003; Elgamal et al. 2005; Popescu et al. 2006) was incorporated in order to simulate free field lateral boundaries away from the pile. This method reproduces essentially the kinematic response of the laminar boxes, used in centrifuge and shaking table experiments, by enforcing equal horizontal and vertical displacements at opposite boundary nodes. In theory, its main drawback is that outwards propagating waves are reflected at the lateral boundaries and consequently they may affect the numerical results. However, such effects are minimal for the highly non-linear problem examined herein, as most of the energy transmitted through the reflected waves is absorbed by the large hysteretic damping of the liquefied sand. Note that the typical tied-node formulation had to be properly modified in the present study, in order to take into account that the ground surface is inclined yielding a hydrostatic pore pressure surplus at the down slope free field boundary.

The numerical analyses were performed for drilled, as well as, for driven piles. The associated stress and volume changes in the soil were simulated based on Vesic's (1972) analytical methodology for the problem of cylindrical cavity expansion which was programmed and implemented to FLAC3D through a FISH function. The various parameters included in Vesic's equations (mainly the volumetric response of the soil) were calibrated through a series of parametric analyses that simulated the expansion of a cylindrical cavity for various soil slices along the pile. After the FISH function is called, just before the application of dynamic loading, the kinematic inconsistency near the ground surface (passive wedge vs. cavity expansion) is identified by the code, leading to the development of upward displacements and the formation of the passive wedge in order to establish equilibrium. The accuracy of this semi-analytical procedure was verified based on results from numerical analyses that fully simulated the problem of pile installation in sands. It was thus observed that this hybrid methodology may decrease drastically the computational cost, with negligible effects on the accuracy of the predictions.

Details on the novel simulations of pile installation effects and tied node boundaries for inclined ground, are provided by Chaloulos (2012) and Chaloulos et al. (2013).

3 Numerical methodology verification

The numerical methodology described in the previous section was consequently used to simulate the centrifuge test performed by González et al. (2009) at RPI. The purpose of the simulation is both to verify the methodology's capacity to capture the basic response patterns observed in the experiment, and also to calibrate the methodology in terms of the permeability coefficient, a soil variable that is not well defined for liquefied soil conditions. Note that, in the following presentation, all dimensions and measurements are given in prototype scale.

Figure 2a shows the centrifuge test set up. Soil consists of a 6 m thick layer of Nevada sand, placed at a relative density of $D_r = 40\,\%$, overlying a 2 m thick non-liquefiable layer

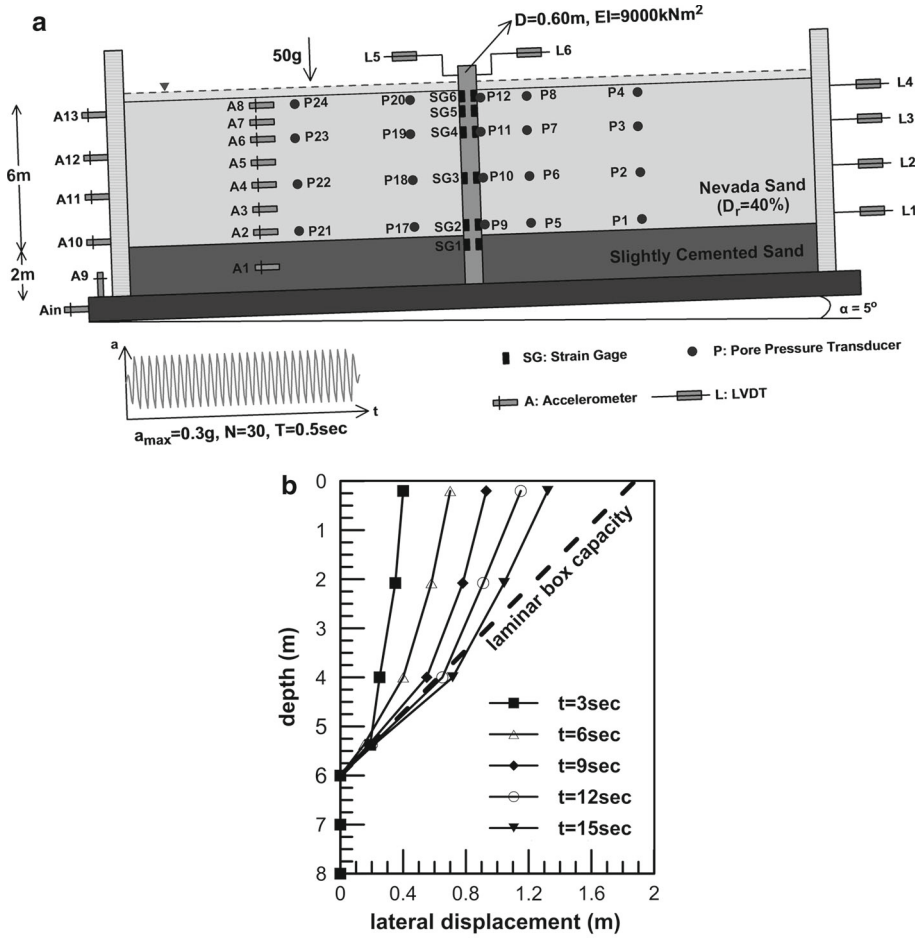

Fig. 2 **a** Setup and Instrumentation used in the experimental model (prototype units) **b** variation of lateral displacement with depth measured at various time instances (after González et al. (2009))

of slightly cemented sand. The laminar box container is inclined at an angle of five (5) degrees relative to the horizontal, in order to simulate an infinite mild ground slope. The pile has a diameter of D = 0.60 m and a bending stiffness EI = 9000 kNm^2, while a sinusoidal excitation of 30 cycles with period T = 0.5 s and peak acceleration a_{max} = 0.30 g is applied at the base of the container. The test was performed under a 50 g centrifugal acceleration, and the system response was monitored by densely placed instrumentation consisting of strain gauges, pore pressure transducers, accelerometers and linear variable differential transducers (LVDTs).

Figure 2b shows the variation of lateral displacement with depth measured at various time instances during the test and compares it to the maximum lateral displacement that is allowed by the rings of the laminar box container (heavy dashed line). It can be observed that the ultimate displacement capacity of the box is reached at t = 3 s at the depth of z = 5.5 m and at approximately t = 6 s for the depth of z = 4 m. Thus, it is speculated that all test measurements beyond t = 6 s may have been affected by this artificial constraint of free field displacements and should be treated with caution.

The mesh created to simulate the test is similar to that in Fig. 1. Following the geometry of the laminar box, the grid is 35.5 m long, 9 m wide and 8 m tall. Along the vertical axis, the mesh is divided into 16 zones of 0.5 m height each, while the horizontal width of the zones starts from 0.30 m at the pile–soil interface and progressively increases with the distance from the pile. Note that this mesh discretization was verified through a number of sensitivity analyses.

The liquefiable Nevada Sand response was simulated with the NTUA Sand model whose parameters have been calibrated for the specific type of sand (Andrianopoulos et al. 2010). The void ratio was set equal to e = 0.74, corresponding to $D_r = 40\,\%$ relative density, while the following scenarios were considered for the permeability coefficient of the sand:

(a) **Static Permeability** k = 6.6e−5 m/s, determined from constant head permeability tests under 1 g gravitational acceleration (e.g. Arulmoli et al. 1992)
(b) **Dynamic Permeability** k = 2.1e−5 m/s. This reduced value has been proposed by Liu and Dobry (1997), in order to take into account the alternating flow direction within the pores of the sand skeleton during shaking.
(c) **Variable permeability**, as proposed by Shahir et al. (2012), in order to take into account that pore pressure build-up and liquefaction cause soil particles to lose full contact leading to the creation of additional flow paths which increase the apparent permeability coefficient:

$$\frac{k_b}{k_{ini}} = 1 + (a - 1)\, r_u^{\beta} \tag{1}$$

In Eq. 1 k_b denotes the applicable value of the permeability coefficient and $k_{ini} (= 2.1 \times 10^{-5}$ m/s) denotes the dynamic value of the permeability coefficient at the onset of shaking, when $r_u = 0$. Based on Shahir et al., the constants in the above relationship were taken as $\alpha = 10$ and $\beta = 1$.

The cemented sand was assumed to behave as a linear elastic material with Poisson's ratio $\nu = 0.33$ and elastic (small strain) shear modulus $G_o = 120000$ kPa. The G_o value corresponds to the elastic stiffness of clean Nevada sand, at the same Relative Density and confining stress levels, multiplied by a factor of two (2) to take into account cementation. This approach for the modulus definition of the cemented soil is based on various studies (Acar and El-Tahir 1986; Saxena et al. 1988; Sharma and Fahey 2003; Schnaid et al. 2001) which suggest that cementation may grossly double the stiffness compared to the same un-cemented soil.

Finally, the pile was considered elastic, as no plastic hinges were developed during the tests. The elastic constants were selected so as to yield a flexural stiffness $EI = 9000$ kNm^2. Interface elements were placed between the pile and the soil to allow for slip and separation. These interfaces were assumed to have zero cohesion, and two possible values of friction angle, $\delta = 1/2\,\varphi$ or $\delta = \varphi$, where φ is the friction angle of the soil. According to González et al. (2009), sand grains were glued to the outer part of the pile, so that the friction of the interface is expected to be closer to that of the sand. Still, both above scenarios were considered, in order to reduce the uncertainty with regard to δ, and also investigate its effect on the model response.

Given the above objective uncertainties with regard to soil permeability and friction angle of the interface, a total of six (6) analyses had to be performed in order to fit the experimental results in a rational way. The basic input parameters of each analysis are summarized in Table 1.

Figure 3a to 3c show the variation with depth of free field displacements at the end of shaking for the aforementioned three (3) different permeability scenarios. Experimental data

Table 1 Summary of the analyses performed for the verification of the numerical methodology

α / α	Permeability, k ($\times 10^{-5}$ m/s)	Interface friction (δ / φ)*
1	6.6	0.5
2	6.6	1.0
3	2.1	0.5
4	2.1	1.0
5	$2.1 \cdot (1 + 9r_u)^{**}$	0.5
6	$2.1 \cdot (1 + 9r_u)^{**}$	1.0

* (δ / φ): Ratio of interface friction over soil friction angle
** Variable permeability with excess pore pressure ratio, r_u

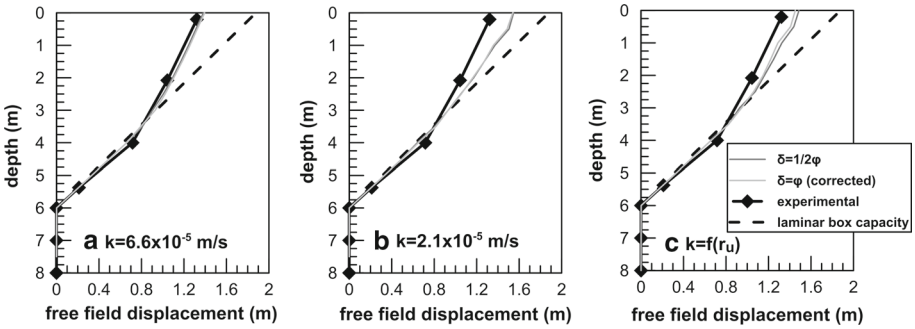

Fig. 3 Experimental and numerical free-field displacement profiles with depth at the end of shaking for **a** k = 6.6e−5 m/s, **b** k = 2.1e−5 m/s and **c** k = f(r_u)

are shown with the black continuous line, while numerical predictions are shown with the dark gray line for $\delta = 1/2\,\varphi$ and the light gray line for $\delta = \varphi$. The black dashed line corresponds to the ultimate horizontal displacement of the laminar box. Taking into account the limited capacity of the laminar box to deform laterally, the numerical predictions $y_{ff}(h)$ were corrected as follows:

$$y_{ff}(h) = \int_0^h \gamma(h) \cdot dh \tag{2}$$

where h is the height above the bottom of the liquefiable layer and $\gamma(h)$ is the numerically computed shear strain at h. Due to the limited angular distortion of the laminar box, it was further assumed that $\gamma(h)$ in the above equation cannot exceed the maximum shear strain that can be developed in the laminar box, i.e. $\gamma(h) \leq \gamma_{ult} \approx 33\,\%$. The corrected numerical displacements are in fairly good agreement with the experimental data, mainly for the k = 6.6e−5 m/s and the k = f(r_u) cases, while the assumed interface friction angle does not seem to affect the comparison.

In a similar fashion, Fig. 4 compares numerically predicted and recorded pile bending moments. Note that, due to the previously discussed laminar box limitations, the comparison is not shown at the end of shaking, but for t = 6 s when the constraints imposed at the lateral boundaries of the box have not been yet mobilized. For this case, the optimum comparison is achieved for the k = 6.6e−5 m/s and the k = 2.1e−5 cases, as well as for interface friction angle $\delta = \varphi$.

According to the comparisons presented so far, an optimum overall fit of the test results is achieved for $\delta = \varphi$, a conclusion which is consistent with the description of pile preparation

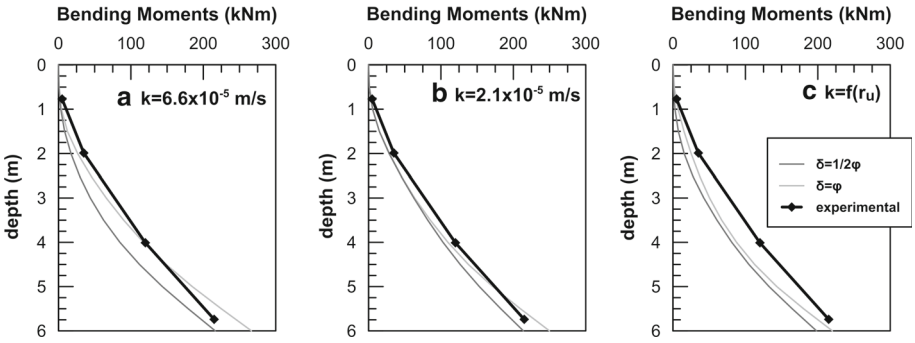

Fig. 4 Experimental and numerical pile bending moments for t = 6 s for **a** k = 6.6e−5 m/s, **b** k = 2.1e−5 m/s and **c** k = f(r_u)

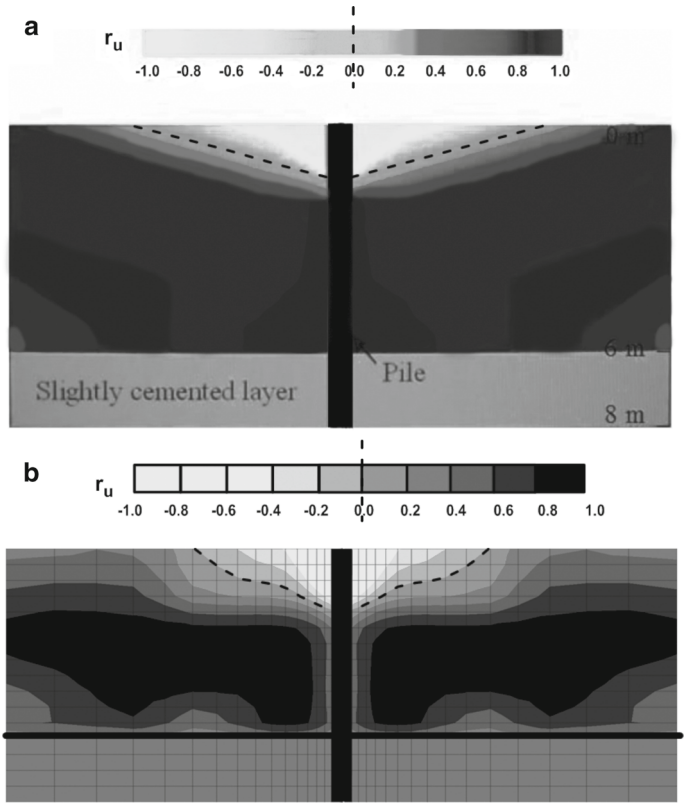

Fig. 5 Experimental measurements (**a**) and numerical predictions (**b**) of excess pore pressure ratio contours at the end of shaking

with sand grains glued on its outer face, and for k = 6.6e−5 m/s. For the above values of the permeability coefficient and interface friction, Fig. 5 compares the contours of excess pore pressure ratio at the end of shaking that were obtained from the test (Fig. 5a) and from the numerical analysis (Fig. 5b). It can be observed that the numerical analysis reproduces fairly well the experimental pattern of pore pressure development, namely that partial or

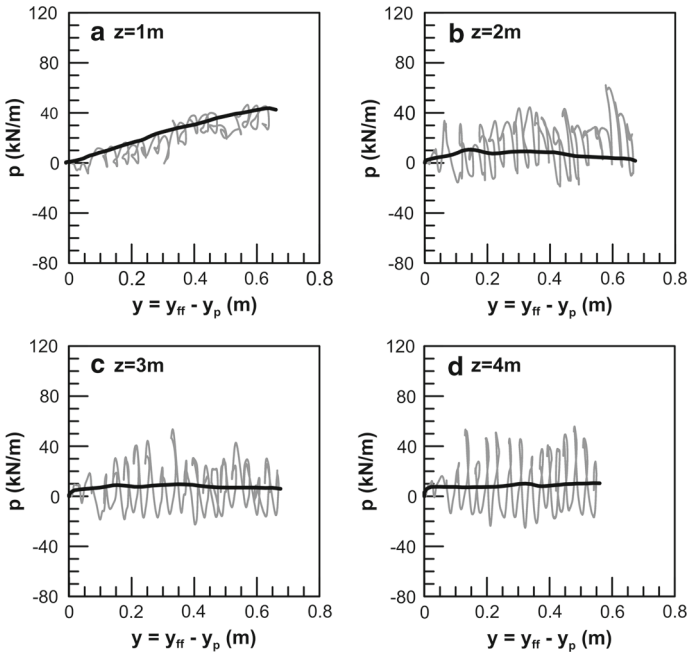

Fig. 6 Experimental and numerical p–y curves for k = 6.6e−5 m/s and $\delta = \varphi$[y_{ff}: soil displacement at the free field; y_p: pile displacement]

complete liquefaction (i.e. $r_u \approx 0.50 \div 1.00$) takes place at large depths and at the free field, while significant dilation (i.e. $r_u < -0.50$) occurs near the top of the pile, leading to the formation of an inverted conical zone of high negative excess pore pressures. This is an important observation, as this response pattern is overlooked by current empirical methods for the computation of the subgrade reaction, despite its detrimental effect on pile response.

Finally, Fig. 6 illustrates the comparison between experimental p–y curves (black line), back-calculated from the bending moments after the cyclic component was filtered out, and the respective non-filtered numerical predictions (gray line), at different depths along the pile. In all cases the experimental curves fall within the range defined by the cyclic and permanent component of the numerical curves. It can be further observed that the response patterns recorded in the test are correctly predicted in the analyses. Namely, soil pressures are larger near the surface (due to soil dilation), while at deeper elevations they obtain a residual value which remains approximately constant with depth.

4 Factors affecting ultimate pressure of laterally spreading soils

4.1 Interpretation of numerical p–y predictions

In the present study, practice oriented p–y curves are obtained by an overall average fitting of the relevant numerical predictions by means of the following hyperbolic function:

$$p = \frac{y_{rel}}{\frac{1}{k_{ini,liq}z} + \frac{y_{rel}}{p_{ult,liq}}} \tag{3}$$

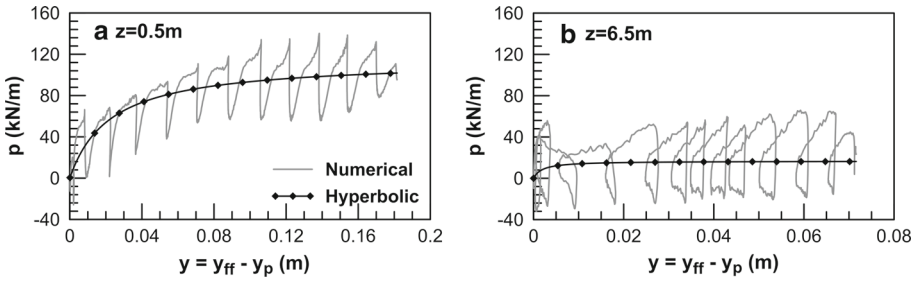

Fig. 7 Adjustment of a hyperbolic curve on the numerically obtained p–y curve for the estimation of ultimate soil pressure

where p is the soil reaction [kN/m], y_{rel} is the relative displacement between the pile and the free field soil [m], $k_{ini,liq}$ is the gradient with depth of the initial subgrade modulus of the liquefied soil [kN/m^3] and $p_{ult,liq}$ is the associated ultimate soil pressure [kN/m].

After trying different approaches, it was found that the most consistent average fit of the numerically predicted p–y curves was obtained assuming that $k_{ini,liq}$ is equal to one half of the initial stiffness for the "dry" soil, i.e.:

$$k_{ini,liq} = 1/2 k_{ini,firm} \tag{4}$$

where the $k_{ini,firm}$ values are obtained from the static p–y analyses obtained at earlier stages of the project (Chaloulos 2012), using the same type of analyses but for "dry" soil conditions. This is clearly a simplification regarding the $k_{ini,liq}$ estimation. However, it was adopted here following the observation that the ultimate soil pressure is reached relatively early during loading, and consequently the initial stiffness of the p–y curve is of secondary importance, relative to the ultimate pressure, for the prediction of pile response.

Typical p–y curves obtained with the above procedure are shown in Fig. 7a, b, for two (2) typical p–y curves obtained from the reference numerical analysis. This procedure was consequently applied to all eighteen (18) analyses of this study. For each analysis, $k_{ini,liq}$ and $p_{ult,liq}$ values were obtained for eight (8) different depths along the pile, leading to the calculation of 144 pairs of values.

4.2 Mechanisms affecting the ultimate p–y resistance

Figure 8a shows the variation with normalized depth z/D of the ultimate pressure ratio $p_{ult,liq}/(\sigma'_{vo}\, D)$, as obtained from the results of the baseline analysis, while Fig. 8b shows the corresponding variation of the average excess pore pressure ratio in the upstream and downstream areas right next to the pile ($r_{u,pile} = \Delta u_{pile}/\sigma'_{vo}$) at the end of shaking. Comparison of the two figures leaves little doubt that the ultimate soil pressure is directly related to the development of pore pressures close to the pile.

Namely, the excess pore pressure ratio $r_{u,pile}$ in Fig. 8a takes large negative values close to the surface and gradually increases with depth, reaching an almost constant positive value of $r_{u,pile} \approx 0.70$–0.75. Note that the dilative response of the soil at the upper part of the pile can be attributed to the small stresses, as well as, to the large relative pile–soil displacements. Except from dilation effects, these data indicate that complete liquefaction never occurs near the pile. On the other hand, the normalized ultimate soil pressure $p_{ult,liq}/(\sigma'_{vo}\, D)$ in Fig. 8b is large close to the ground surface and gradually decreases with depth. It is also interesting to note that there is an upper limit to the dilation-induced large values of normalized soil

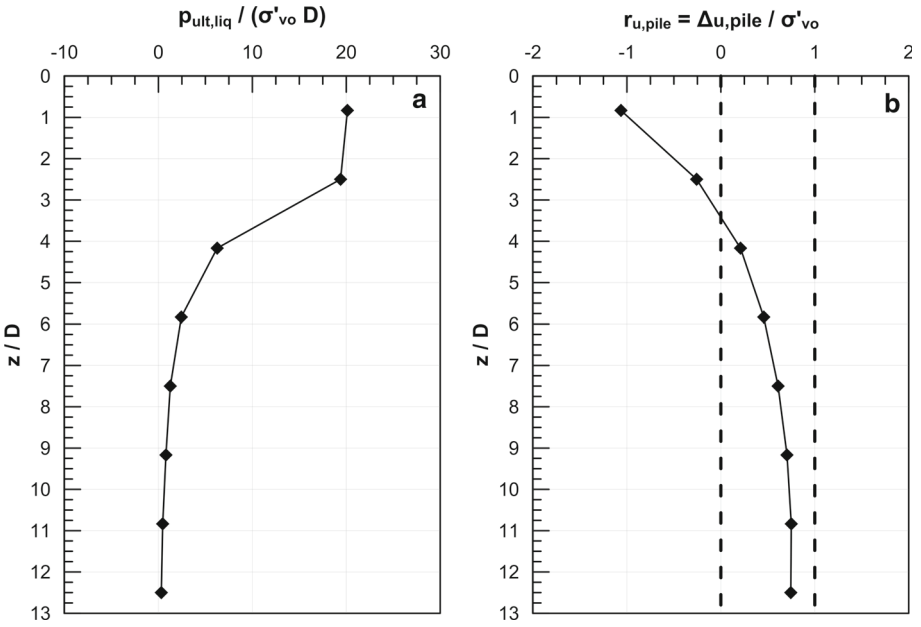

Fig. 8 Variation of **a** normalized ultimate soil pressure $p_{ult,liq}/(\sigma'_{vo}\,D)$ and **b** excess pore pressure ratio near the pile, $r_{u,pile}$ with depth

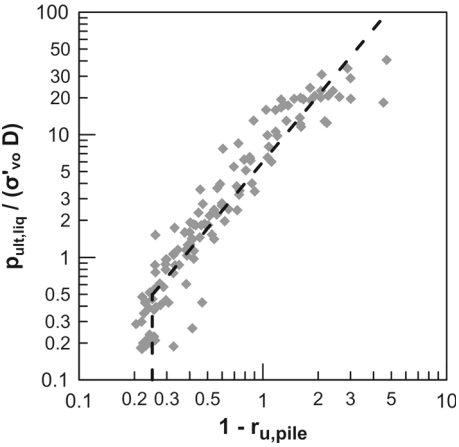

Fig. 9 Relation between normalized ultimate soil pressure and average excess pore pressure ratio next to the pile

pressure, which are observed close to the ground surface, so that the value of $p_{ult,liq}/(\sigma'_{vo}\,D)$ is practically constant with depth for the first few pile diameters. The fact that the ultimate pressure ratio does not continue to increase until the ground surface can be attributed to drainage and dissipation of the negative excess pore pressures towards the free surface.

To further investigate the correlation between ultimate pressure and pore pressure development near the pile, Fig. 9 plots the $p_{ult,liq}/(\sigma'_{vo}\,D)$ values against $1 - r_{u,pile}$, for the whole set of numerical analyses performed herein. Observe that all data points form a remarkably narrow band, indicating a unique relation between the ultimate pressure of the liquefied soil and the average excess pore pressure in the vicinity of the pile. This finding is the key for

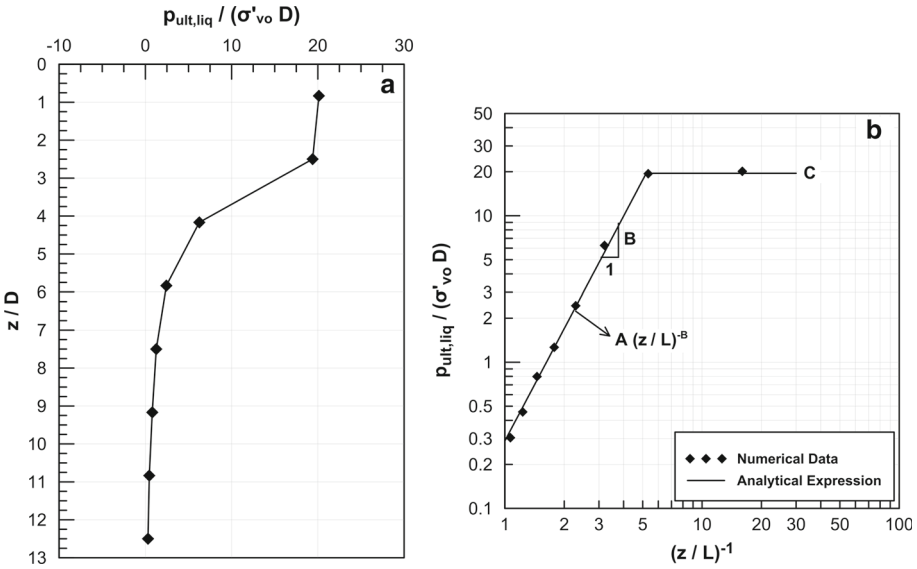

Fig. 10 Variation of normalized ultimate pressure, $p_{ult,liq}/(\sigma'_{vo}\,D)$ with **a** normalized depth and **b** the inverse of normalized vertical effective stress, $1/(\sigma'_{vo}/p_a)$ for the basic analysis

understanding the mechanism that controls the interaction between the pile and the liquefied soil. Nevertheless, its practical use is unfortunately limited since excess pore pressures in the immediate vicinity of the pile are drastically different than in the free field and cannot be predicted by simple analytical means. Thus, as a first step towards an improved p–y methodology for liquefied soils, our attention was alternatively focused on the correlation of the ultimate pressure to known in advance basic soil, pile and excitation parameters which are expected to affect excess pore pressure build-up near the pile.

4.3 Parametric evaluation of ultimate p–y Resistance

Following a number of trials, it was found that the ultimate pressure ratio may be related to the depth over pile length ratio z/L as:

$$\frac{p_{ult,liq}}{\sigma'_{vo}D} = A\left(\frac{z}{L}\right)^{-B} \leq C \tag{5}$$

The physical meaning of the above relation is realized from Fig. 10b, where the basic variables are correlated in a double logarithmic scale. This figure indicates that, the normalized ultimate soil pressure increases log-linearly with decreasing depth, until it reaches a constant peak value. To this extent, coefficient A corresponds to the normalized pressure at the tip of the pile (z = L), i.e. it is representative of soil pressure at relatively large depths, where the response is contractive, characterized by values of excess pore pressure ratio close to unity. On the other hand, coefficient C is representative of soil pressure at small depths, where large dilation occurs, resulting in large soil pressure values. Finally, coefficient B represents the rate of transition with depth, from the state of positive excess pore pressures and small pressure values at large depths (i.e. $p_{ult,liq} \sim A$), to that of negative excess pore pressures and large soil pressures at shallow depths (i.e. $p_{ult,liq} \sim C$).

In the sequel we focus upon coefficients A and C, as they are representative of the limits of ultimate pressure variation along the pile. Based on the results of the parametric numerical

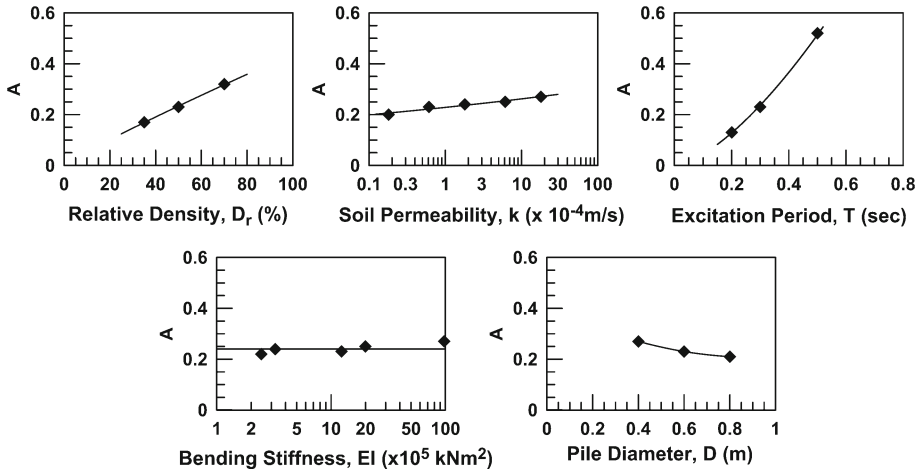

Fig. 11 Variation of coefficient A with the different soil, pile and excitation characteristics

analyses, Figs. 11 and 12 summarize the effect on coefficients A and C of the following basic problem variables: relative density and permeability coefficient of the sand, excitation period, as well as bending stiffness and pile diameter. At a first glance, observe that all above parameters have a measurable effect on A and C, indicating that the ultimate liquefied soil pressure is a multi-variable quantity and not merely relative density dependent. In more detail, the effect of each parameter is briefly discussed and potentially explained in the following.

Effect of Relative Density, D_r: Coefficient A increases while coefficient C decreases with D_r, The effect on A is expectable since this coefficient reflects ultimate pressure for large positive values, i.e. nearly at free field liquefaction, which is widely known to be larger for more dense soils. The effect on C is explained if one considers that liquefaction induced lateral ground displacements, and consequently the relative displacement between the pile and the soil, are less for more dense sands. As a result, dilation phenomena are less severe and the ultimate soil pressure at the top of the pile is reduced accordingly. Of course, one may argue that more dense soils are more dilative as well. However, it appears that the mechanism of negative excess pore pressure accumulation due to large displacements and straining prevails.

Effect of Soil Permeability, k: Coefficient A appears to slightly increase for larger k values, as excess pore water pressures at the pile tip decrease due to flow towards the negative excess pore pressures at the pile head. On the contrary, coefficient C drastically decreases with k, as pore water flows faster towards the area around the pile head that exhibits dilation, hence suppressing the associated negative excess pore pressures and decreasing ultimate soil pressure.

Effect of Excitation Period, T: When T is increased, pore water at large depths is given more time within each cycle to flow towards the negative excess pore pressure field that develops close to the pile head. Hence, positive excess pore pressures at large depths are decreased, leading to larger values of the ultimate soil pressure and coefficient A. For the same reason, negative excess pore pressures close to the pile head are (algebraically) increased, leading to lower values of the ultimate soil pressure and coefficient C.

Effect of Pile Bending Stiffness, EI: The bending stiffness of the pile seems to affect coefficient C only. Namely, interpreting the trend of the data points, C and the ultimate

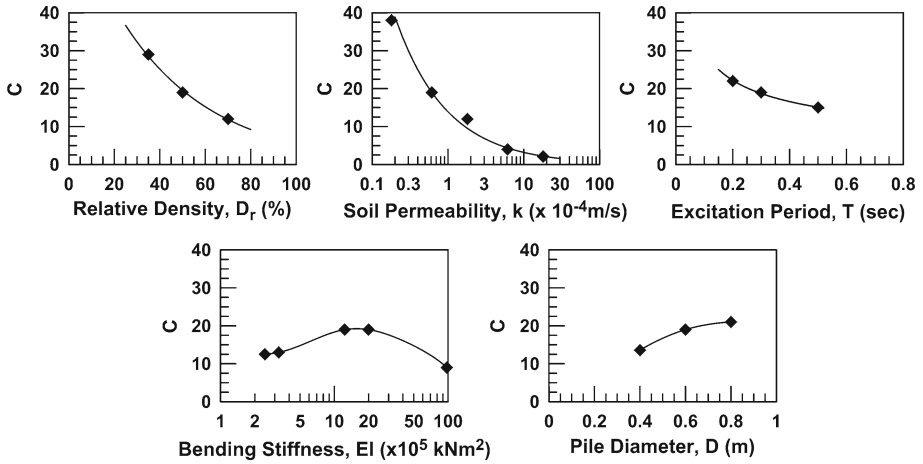

Fig. 12 Variation of coefficient C with the different soil, pile and excitation characteristics

soil pressure at the pile top initially increase with EI but subsequently decrease after reaching a peak value. The following are speculated with regard to this effect: (a) Very flexible piles practically follow the movement of the soil, yielding small relative pile–soil displacements, and, hence small dilation and small soil pressure. (b) As the flexural stiffness of the pile increases, relative displacements increase leading to the development of negative excess pore pressures and increased soil pressure. (c) After a certain EI value, i.e. for very stiff piles, relative displacements are again reduced due to "pinning effects" of the piles on the laterally spreading ground, causing the soil pressure to decrease again.

Effect of Pile Diameter, D: Pile diameter does not appear to have a significant effect on coefficient A, while coefficient C appears to increase with pile diameter. This effect can be justified by observing Fig. 13. Namely, as diameter increases dilation phenomena become more intense, with excess pore pressures becoming more negative near the pile head. This response causes soil pressure to increase. However, the reasons for this more dilative response are not presently clear, and a possible explanation can only be based on speculation. For instance, it is possible that as the diameter increases the length of drainage paths also increase, causing the dissipation of pore pressures to evolve much more slowly. Also, the increase in the thickness of the sand layer (as described earlier, all mesh dimensions were scaled based on the change in diameter), resulted in larger free field displacements and possibly in larger pile–soil relative displacements and a more dilative response. In any case, the effect of pile diameter, as well as scale effects in general, deserve further study.

5 Discussion

To evaluate the practical significance and the field of application of the previous findings, numerical predictions are compared to empirical predictions with the recently proposed methods of Brandenberg et al. (2007), Cubrinovski and Ishihara (2007) and Tokimatsu and Suzuki (2009). All these methods draw upon experimental results from centrifuge and large shaking table tests, and do not make any explicit reference to the dilation effects discussed in this paper.

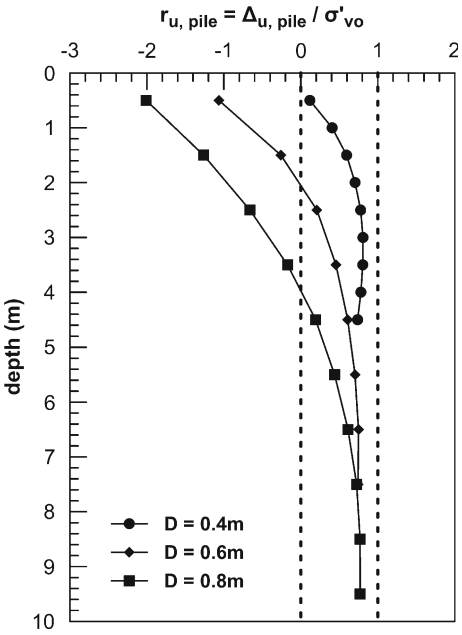

Fig. 13 Variation of excess pore pressure ratio near the pile, $r_{u,pile}$, with depth for the analyses with different pile diameters

The numerical, as well as, the empirical predictions refer to the same case, where an L = 8 m long and D = 0.6 m diameter concrete pile, with bending stiffness EI = 250000 kNm^2, is installed in an 8 m thick uniform Nevada sand layer with $D_r = 50\,\%$ relative density, and is rigidly supported at its base. The friction angle of the soil was taken equal to $\varphi = 33°$ and the buoyant weight as $\gamma' = 9.81$ kN/m^3. Based on the empirical relation by Tokimatsu and Seed (1987), the equivalent SPT blow count for this soil was estimated as $(N_1)_{60-cs} = 44 \times 0.50^2 = 11$.

To explore the effects of dilation at the upper part of the pile, the numerical predictions are shown for two different permeability coefficients of the sand: k = 6.1e−5 m/s, typical for fine sands or silt-sand mixtures, and k = 3.05e−3 m/s, typical of coarse sands or sand-gravel mixtures. Note that the empirical methodologies do not account for permeability effects and consequently the associated predictions remain the same for both values of k. Furthermore, the predictions according to Brandenberg et al. (2007) are drawn as a range, for the lower and the upper bound values of the p–y curve multiplier $m_p = 0.050$ and 0.165, while the predictions by Tokimatsu and Suzuki (2009) are drawn for a reduction multiplier value equal to $\beta \approx 0.10$(for $z < 10$ m).

Focusing first upon the variation with depth of the normalized ultimate soil pressure, inspection of Fig. 14a reveals that:

- When the expected dilation is not significant, i.e. for medium and large depths and large permeability coefficients, the numerical predictions fall within the range of empirical predictions.
- On the contrary, when significant dilation is expected, i.e. for shallow depths and low permeability coefficients, the numerical predictions increase drastically and become approximately one order of magnitude larger than the empirical ones.

The above observations come in support of the basic argument of González et al. (2009), namely that dilation effects may have been masked in the scaled model experiments that were

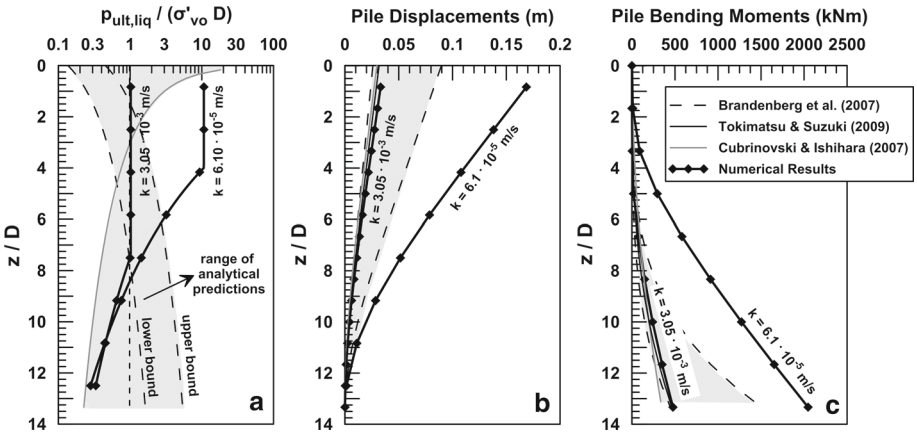

Fig. 14 Comparison of analytical predictions and numerical results in terms of **a** ultimate soil pressure, **b** pile deflections and **c** bending moments

used to obtain current empirical methods due to the use of water, instead of a higher viscosity fluid, to saturate the liquefiable sand. Furthermore, they imply that current empirical methods perform reasonably well for high permeability coarse sands and sand-gravel mixtures, but may underestimate significantly the liquefied soil pressures, as well as the associated pile deflections and bending moments for fine sands and silt-sand mixtures.

The aforementioned dilation effects on pile response are further explored in Fig. 14b, c which compare numerical and empirical predictions of pile deflections and bending moments. It is thus verified that numerical and empirical predictions are in reasonably good agreement for high permeability soils and negligible dilation effects, while the former are 2.5–3.0 times larger for low permeability and high dilation conditions.

Note that in Chaloulos et al. (2014), the above findings are further investigated with the aid of additional numerical analyses, while multi-variable empirical relations for the ultimate soil pressure of the liquefied soil, which account consistently for the previously discussed dilation effects, are proposed.

Finally, it is of interest to explore whether the present findings can be extended to different soil profiles, with special attention given to the common case where an impermeable clay cap lays over the liquefied sand layer. In such profiles, dilation effects are controlled by two competing mechanisms: drainage towards the ground surface is suspended, thus intensifying dilation effects close to the pile top, but at the same time relative pile–soil displacements are reduced, yielding opposite results on anticipated dilation effects.

Acknowledgments In support of our research, Itasca Inc. has granted free use of FLAC3D (4.0) through Educational Loan S/N 242-001-0165. This contribution is gratefully acknowledged.

References

Acar YB, El-Tahir E-TA (1986) Low strain dynamic properties of artificially cemented sand. J Geotech Eng 112(11):1001–1015

Andrianopoulos KI, Papadimitriou AG, Bouckovalas GD (2010) Bounding surface plasticity model for the seismic liquefaction analysis of geostructures. Soil Dyn Earthq Eng 30(10):895–911

Arulmoli K, Muraleetharan KK, Hossain MM, Fruth LS (1992) VELACS: verification of liquefaction analyses by centrifuge studies; Laboratory Testing Program—Soil Data Report. Research Report, The Earth. Technology Corporation

Brandenberg SJ, Boulanger RW, Kutter BL, Chang D (2007) Static pushover analyses of pile groups in liquefied and laterally spreading ground in centrifuge tests. J Geotech Geoenviron Eng 133(9):1055–1066

Chaloulos YK (2012) Numerical investigation of pile response under liquefaction and ground lateral spreading. PhD Thesis, Dept of Civil Engineering, NTUA, Athens

Chaloulos YK, Bouckovalas GD, Karamitros DK (2013) Pile response in submerged lateral spreads: common pitfalls of numerical and physical modeling techniques. Soil Dyn Earthq Eng 55:275–287

Chaloulos YK, Bouckovalas GD, Karamitros DK (2014) Analysis of liquefaction effects on ultimate pile reaction to lateral spreading. J Geotech Geoenviron Eng. doi:10.1061/(ASCF)GT.1943-5606.0001047

Cubrinovski M, Ishihara K (2007) Simplified analysis of piles subjected to lateral spreading: parameters and uncertainties. In: Pittilakis K (ed) 4th International conference on earthquake geotechnical engineering, Thessaloniki, Greece

Elgamal A, Lu J, Yang Z (2005) Liquefaction-induced settlement of shallow foundations and remediation: 3D numerical simulation. J Earthq Eng. 9(SPEC. ISS.):17–45

Ghosh B, Madabhushi SPG (2003) A numerical investigation into effects of single and multiple frequency earthquake motions. Soil Dyn Earthq Eng 23(8):691–704

González L, Abdoun T, Dobry R (2009) Effect of soil permeability on centrifuge modeling of pile response to lateral spreading. J Geotech Geoenviron Eng 135(1):62–73

Karamitros DK (2010) Development of a numerical algorithm for the dynamic elastoplastic analysis of geotechnical structures in two and three dimensions. PhD Thesis, Dept of Civil Engineering, NTUA, Athens

Liu L, Dobry R (1997) Seismic response of shallow foundation on liquefiable sand. ASCE J Geotech Geoenviron Eng 123(6):557–566

Papadimitriou AG, Bouckovalas GD (2002) Plasticity model for sand under small and large cyclic strains: a multiaxial formulation. Soil Dyn Earthq Eng 22(3):191–204

Popescu R, Prevost JH, Deodatis G, Chakrabortty P (2006) Dynamics of nonlinear porous media with applications to soil liquefaction. Soil Dyn Earthq Eng 26(6–7):648–665

Saxena SK, Avramidis AS, Reddy KR (1988) Dynamic moduli and damping ratios for cemented sands at low strains. Can Geotech J 25(2):353–368

Schnaid F, Prietto PDM, Consoli NC (2001) Characterization of cemented sand in triaxial compression. J Geotech Geoenviron Eng 127(10):857–868

Sharma SS, Fahey M (2003) Degradation of stiffness of cemented calcareous soil in cyclic triaxial tests. J Geotech Geoenviron Eng 129(7):619–629

Tokimatsu K, Seed HB (1987) Evaluation of settlement in sands due to earthquake shaking. J Geotech Eng 113(8):861–878

Tokimatsu K, Suzuki H (2009) Seismic soil-pile-structure interaction based on large shaking table tests. In: Kokusho T, Tsukamoto Y, Yoshimine M (eds) Performance-based design in earthquake geotechnical engineering. Taylor & Francis, London

Vesic AS (1972) Expansion of cavities in infinite soil mass. ASCE J Soil Mech Found Div 98(SM3):265–290